Nanoscale

RSC Publishing

PAPER

View Article Online
View Journal | View Issue

Bio-nanohybrids of quantum dots and photoproteins facilitating strong nonradiative energy transfer†

Cite this: *Nanoscale*, 2013, **5**, 7034

Urartu Ozgur Safak Seker,§,‡*[ab] Evren Mutlugun,‡[ab] Pedro Ludwig Hernandez-Martinez,[ab] Vijay K. Sharma,[b] Vladimir Lesnyak,¶[c] Nikolai Gaponik,[c] Alexander Eychmüller[c] and Hilmi Volkan Demir*[ab]

Utilization of light is crucial for the life cycle of many organisms. Also, many organisms can create light by utilizing chemical energy emerged from biochemical reactions. Being the most important structural units of the organisms, proteins play a vital role in the formation of light in the form of bioluminescence. Such photoproteins have been isolated and identified for a long time; the exact mechanism of their bioluminescence is well established. Here we show a biomimetic approach to build a photoprotein based excitonic nanoassembly model system using colloidal quantum dots (QDs) for a new bioluminescent couple to be utilized in biotechnological and photonic applications. We concentrated on the formation mechanism of nanohybrids using a kinetic and thermodynamic approach. Finally we propose a biosensing scheme with an ON/OFF switch using the QD–GFP hybrid. The QD–GFP hybrid system promises strong exciton–exciton coupling between the protein and the quantum dot at a high efficiency level, possessing enhanced capabilities of light harvesting, which may bring new technological opportunities to mimic biophotonic events.

Received 21st March 2013
Accepted 19th May 2013

DOI: 10.1039/c3nr01417g

www.rsc.org/nanoscale

Introduction

Bioluminescence is a biological activity of different organisms ranging from bacteria to plants.[1–4] Unlike the photoluminescence and fluorescence, bioluminescence is a cold body radiation triggered by a chemical reaction in the biological organism. In bioluminescence, a molecule is produced at the excited state, which finally emits a photon during relaxation. Among those molecules utilized during bioluminescence, the green fluorescent protein, a well-characterized photoprotein, which has been widely used in biolabeling, is well known.[5,6]

GFP and GFP mutants based on Förster-type resonance energy transfer (FRET) were utilized to track a targeted biological event within a living cell, where the FRET processes between the GFP and its mutants are utilized as reporters.[7–9] Naturally occurring systems exhibit their own strength by means of physical, mechanical and optical properties. They were formed after a long evolutionary process, which gave them strength and flexibility. Therefore, photoproteins are unique owing to simplicity of their synthesis and optical adjustability through genetic engineering tools. On the other side, technologically improved approaches can solve an actual problem that nature does not necessarily need to deal with. At this stage, nanocrystals were synthesized and being offered for utilization in technological applications.[10–12] A hybrid of these two components offers new possibilities; by using the unique optical properties of QDs and introducing the flexibility, genetic tenability and biocompatibility of GFP, a promising hybrid system for biomedical imaging applications and biochemical applications can be favored. Initial studies have successfully presented a bionanohybrid approach for the assembly of protein/photoprotein–QD conjugates.[10,13–16] However, investigation of the nanohybrid formation mechanism by means of the kinetics and thermodynamics of the interaction of the QDs with proteins will increase the control over the assembly. Such an investigation may contribute to the understanding of molecular interactions for future engineering of the nanohybrid using tools of biochemistry and materials science.

In this study we propose a route to QD–GFP nanohybrid assembly. Our approach is different from the previous studies in that, instead of the fluorescence intensity measurements that

[a]*Luminous! Center of Excellence for Semiconductor Lighting and Displays, School of Electrical and Electronic Engineering, School of Physical and Mathematical Sciences, Nanyang Technological University, Nanyang Avenue, Singapore 639798, Singapore*

[b]*Department of Physics, Department of Electrical and Electronics Engineering, UNAM – Institute of Materials Science and Nanotechnology, Bilkent University, TR-06800, Ankara, Turkey. E-mail: volkan@bilkent.edu.tr; urartu@mit.edu*

[c]*Physical Chemistry/Electrochemistry, TU Dresden, Bergstr. 66b, 01062 Dresden, Germany*

† Electronic supplementary information (ESI) available: Details of the quantum dot characterization, GFP-6X-His purification, raw data of XPS analysis of the nanohybrid and TGA raw data. See DOI: 10.1039/c3nr01417g

§ Present address: Massachusetts Institute of Technology, Synthetic Biology Center, 500 Technology Square, NE47-257, Cambridge, MA, USA

‡ These authors have contributed equally.

¶ Present address: Instituto Italiano di Tecnologia, Via Morego 30, 16163 Genova, Italy

need to be normalized regarding the emitting species,[17] and therefore can be deceptive without a calibration; a more accurate method, time resolved fluorescence spectroscopy, was used to follow emission kinetics of the FRET facilitating species. The FRET process was characterized to determine donor and acceptor lifetimes, regardless of the amounts of the FRET facilitating species. The kinetics and thermodynamics of the formation of the nano-bio hybrid structure was investigated to understand how to control the supramolecular interaction within a nanohybrid. Kinetic investigations also led us to determine the distance between each components of the nanohybrid, which was verified theoretically as well. Not only the kinetic analysis but also X-ray photoemission spectroscopy and thermogravimetric analysis were carried out to probe the formation of the GFP–QD nanocomposites. Functional analysis of the GFP–QDs revealed a high FRET efficiency of 70%, and we have showed up to 15-fold enhancement in the emission of the GFP when conjugated with QDs due to the strong excitonic interaction possessing the nonradiative energy transfer. Exploiting the strong nonradiative energy transfer within the nanohybrid, a protease sensor working upon a temperature dependent ON/OFF switch was demonstrated as a tool for temperature based protease sensor applications. In this work, a bottom-up approach for the nanohybrid design, which mimics the aequorin–GFP pair existing in the jellyfish *Aequorea victoria*, with high controllability and adjustability promising a wide range of applicability, is demonstrated.

Experimental section

Preparation of nanocrystals

ZnCdSe quantum dots have been synthesized according to the previously reported work.[18]

Expression and purification of GFP-6X-Histag

The *gfp* gene was first amplified using P1 and P2 primers (see ESI†) carrying NcoI and BamHI restriction sites at their 5′ ends respectively. The P2 primer also contained sequences encoding for the trypsin protease cleavage site (STRTDEG) and Histag (HHHHHH) at its 3′ end. The amplified gene was cloned into a pet11D vector digested with NcoI/BamHI. *Escherichia coli* BL21 strain was transformed with pet11D encoding engineered *gfp*. Purified engineered GFP was attached to the QD surface through coordination with Histag.

Quartz crystal microbalance-dissipation analysis

The interaction of the GFP-6X-His with the QDs was tested using a quartz crystal microbalance Q-Sense E1 (from Q-Sense Company, Frolunda, Sweden). First the surface of the gold QCM-D crystals was activated using cysteamine and then using carbodiimide chemistry, and then QDs were attached to the functionalized sensor surface. After ensuring the attachment of the QDs from the observation of frequency change, the GFP-6X-His was flown on the surface and the change in the frequency shift at varying GFP concentrations was recorded.

Isothermal titration calorimetry

Experiments were carried out using Microcal 200 equipment (GE Healthcare, Austria). Quantum dots at 15 μM concentrations were kept in a titration vessel while the 150 μM GFP-6X-Histag was injected into the QD colloid. The thermal titration was performed at 25 °C and in 0.5× PBS buffer at 500 rpm. ITC data were fitted to a single interaction function using Origin 7 supplied along with the ITC200. Following the runs, the instrument was automatically and manually cleaned with methanol, detergent and DI water.

Time-resolved photoluminescence

Experiments were performed using a PicoQuant Fluo Time 200 time-correlated single photon counting system. A laser diode operating at 375 nm has a repetition rate of 80 MHz with 200 ps width. The lifetimes have been extracted using the data acquisition software PicoHarp 300 with a <10 ps lifetime resolution.

Steady-state photoluminescence and absorption

A Cary Eclipse fluorescence spectrometer and a Cary UV-Vis spectrometer were used in the experiments.

Results and discussions

Kinetic and thermodynamic analysis of GFP–QD nanohybrid formation

In order to investigate the interaction modes between the QDs and GFP, we carried out a quartz crystal microbalance (QCM-D) based affinity analysis where we monitored the binding kinetics of the GFP molecules on the surface decorated with QDs as presented.[19] In this setup, ZnCdSe QDs were first immobilized on the gold surface of the QCM-D sensor by means of carbodiimide mediated covalent bonding. The unfilled parts of the sensor were blocked with 1 mM ethanolamine to prevent the nonspecific attachment of the QDs on the modified sensor surface. Following the coverage of the QCM-D sensor surface, the GFP-6X-His molecule was sent into the flow cell of the QCM-D where the QD functionalized sensors were placed. The adsorption and desorption of the molecules were monitored for five varying concentrations of GFP-6X-His, ranging from 2 to 10 μM. The interaction analysis was carried out using a simple interaction model, which yielded an affinity constant of 0.9 μM, indicating a strong interaction between the GFP-6X-His and QD. QCM-D does not only provide the binding isotherms but also gives the dissipation data of the adsorbed GFP layer on QDs. The dissipation data indicate here that the interaction between the QDs and GFP-6X-His resulted in the formation of a GFP film on top of the QDs without denaturation of the GFP.

Using the dissipation data (Fig. 1a) for fitting to a Voigt viscoelastic model,[20] the thickness of the GFP film was calculated to be as high as ~3 nm (see Fig. 1b). Considering the GFP has a barrel structure composed of sheets and helices with a total diameter of 30 to 40 Å,[21] the results suggest that the GFP-6X-His molecules interact with the QDs *via* the longer side of the barrel, as represented in Fig. 1b. Also, the dissipation change throughout the interaction experiment suggests that the

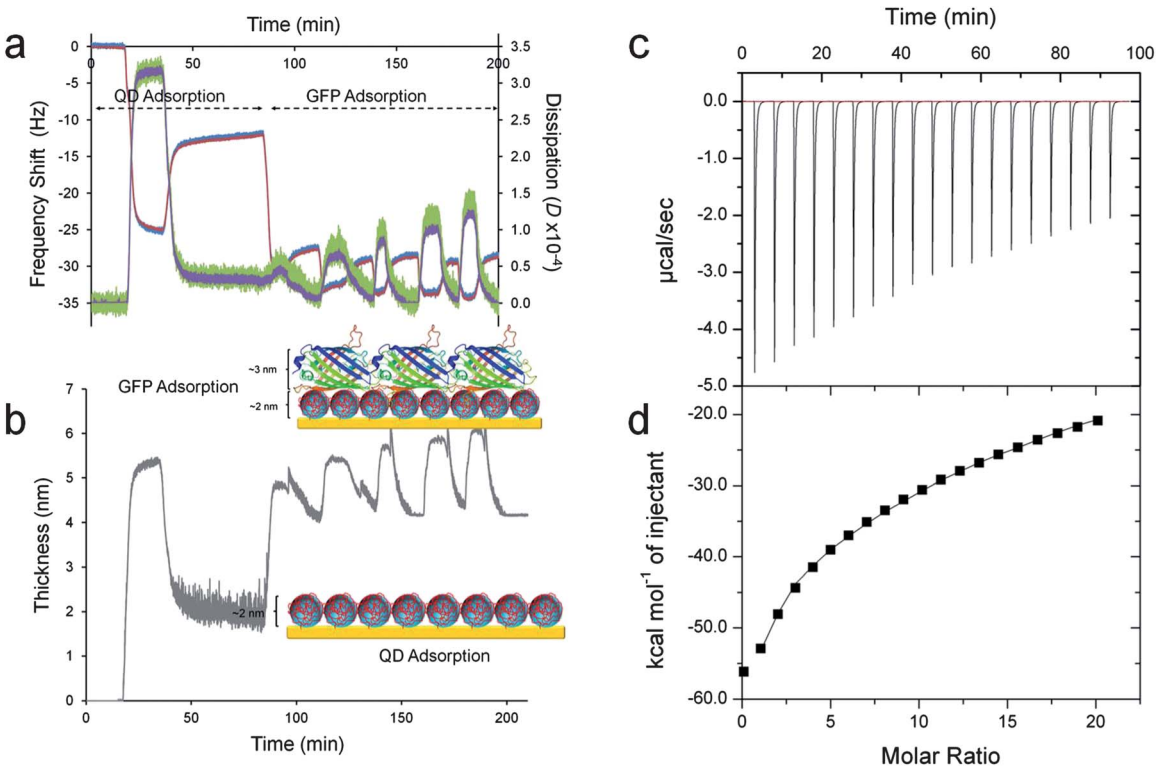

Fig. 1 QCM-D analysis of the binding of QDs and GFP-6X-His in a sequential manner. (a) Frequency shift upon adsorption of quantum dots and GFP-6X-His (blue line) with a viscoelastic model fit (red line) and dissipation change upon adsorption of the nonentities and GFP on a cysteamine modified gold electrode (green line) along with the viscoelastic model fit (purple line). (b) Thickness monitoring of the layer-by-layer assembly of the QDs and GFP-6X-His. (c) ITC titration curves of GFP-6X-His onto QDs after each injection. (d) Calculated area under the ITC titration curves and model fitting of a single interaction model using the software provided along with the instrument.

QD–GFP film entraps water molecules, preventing the GFP from denaturation upon interaction with the semiconductor surface, which otherwise would lead to improper FRET distance between the QD–GFP.

Since the final design of the QD–GFP nanohybrids is water dispersible colloidal entities, besides confirming the thickness of GFP and its affinity on a solid surface, a solution based biophysical approach, isothermal titration calorimetry (ITC) was employed to probe the strength of the interaction between QD–GFP. In the experimental setup GFP-6X-His was injected into the ZnCdSe QD solution placed in a reaction chamber made up of a biologically inert alloy. After each injection of the GFP into the reaction chamber of ITC, released energy upon GFP's interaction with QDs was recorded as given in Fig. 1c. Peak areas were calculated and fitted to an interaction model supplied by Origin software, which is shown in Fig. 1d. From the single mode interaction model, the enthalpy of binding for the QDs and GFP-6X-His was calculated to be -82 kcal mol^{-1}. Although this is a high amount of energy release, we observed a lower affinity desorption constant of 17 μM compared to the QCM-D analysis. This indicates different modes of binding in both experimental cases. The difference in the binding mechanism may arise due to the higher local concentration of QDs in the film as compared to the solution, and these facts may be facilitated by the interaction of the GFP molecules with the QDs. Additionally, through the interaction of the adjacent protein molecules, amounts of proteins adsorbed on the QD surface can be increased.

Although we have strong evidence of the interactions between GFP-6X-His and ZnCdSe QDs, we further investigated the chemical interactions of the GFP with the QDs at the atomic level using the X-ray photoemission spectroscopy (XPS). As presented in XPS data in the ESI,† the high resolution C 1s & O 1s spectra of the GFP, ZnCdSe QDs, and the composite were acquired. Due to the changes in the XPS spectrum of the GFP–QD mixture and the existence of an additional peak compared to the GFP and QD alone, we suspect that the imidazole ring of the histidine tag at the end of GFP gets in contact with the QDs through supramolecular interactions.

Experimental and theoretical analysis of nonradiative energy transfer in the GFP–QD nanohybrid

Energy transfer mediated light harvesting was first performed under steady state conditions. Later, time-resolved photoluminescence measurements were employed to monitor the energy transfer. The steady state measurements demonstrate the effect of the energy transfer from the QDs (D) to GFP (A). As the A/D ratio is increased, we observe a decrease of the emission intensity of the donor QDs, whereas an increase in the acceptor emission is observed as a result of energy feeding from the donor side. A spectral overlap between the emission

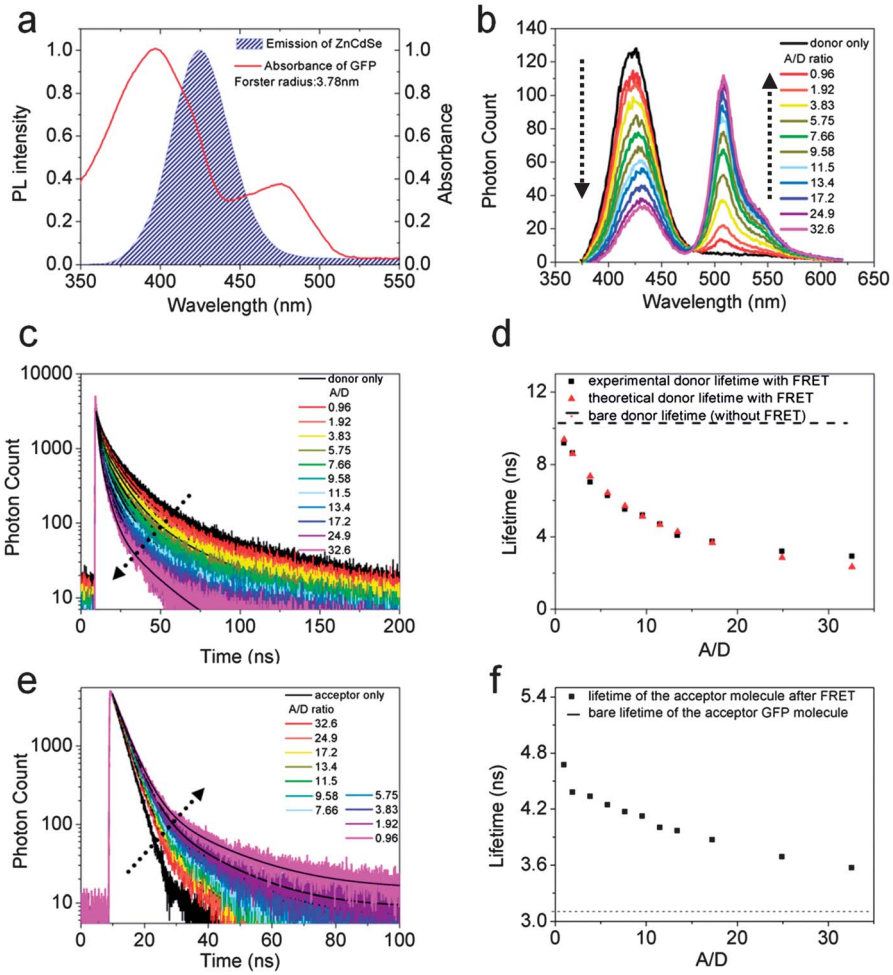

Fig. 2 (a) Spectral overlap of ZnCdSe QDs and GFP, the red line shows the absorption spectrum of the GFP and the blue shadowed area represents the emission spectrum of the ZnCdSe QDs. (b) Photoluminescence spectra of the donor–acceptor QD–GFP system with changing A/D concentration ratio (excitation at 315 nm). (c) Time-resolved photoluminescence decays of the donor, changing with the A/D ratio (at 422 nm). (d) Donor lifetimes, extracted from time-resolved photoluminescence decays, and theoretically predicted, as a function of the A/D ratio. (e) Time-resolved photoluminescence decays of the acceptor changing with the A/D ratio (at 508 nm). (f) Acceptor lifetimes, extracted from time-resolved photoluminescence decays, as a function of the A/D ratio.

of the QDs (with an emission maximum at 422 nm) and the optical absorption of GFP (maxima at 395 nm and 475 nm) was verified to satisfy FRET as presented in Fig. 2a. Steady state fluorescence measurements were performed to monitor any changes in the emission of QDs and GFP before their interactions as well the emission of the nanohybrid structure with the excitation monochromator set at 315 nm. The photoluminescence measurements of the quantum dot-protein composite are shown in Fig. 2b. The enhancement of the pure acceptor emission is extracted from the steady state emission data of the GFP in the presence and absence of the donor QDs.

To demonstrate the excitation of the GFP well beyond its absorption, we chose the excitation wavelength at 315 nm, in order to satisfy the spectral overlap conditions at the expected maximum efficiency (ESI Fig. S5†). The enhancement of the acceptor emission was calculated as a function of the acceptor concentration, and presented as the A/D concentration ratio.

$$\text{Enhancement} = \left[\frac{\int_{480}^{620} I_A^D(\lambda)\mathrm{d}\lambda}{\int_{480}^{620} I_A(\lambda)\mathrm{d}\lambda} - 1 \right] \quad (1)$$

Here, I_A is the intensity of the acceptor GFP in the absence of the donor QDs and I_A^D is the intensity of the acceptor in the presence of the donor. The wavelength interval from 480 to 620 nm was chosen since the emission spectrum of GFP lies within this region. Carrying out the analysis, we observed an enhancement of the acceptor photoluminescence of up to 15 fold corresponding to an A/D ratio of ~5, which is consistent with the geometrical factors given the size of the GFP and the QDs. As the amount of GFP is further increased, the overall enhancement decreases because the system is converging to the case of acceptor only.

Using time-resolved photoluminescence spectroscopy fluorescence emission lifetimes of the donor, the acceptor

and the hybrid were monitored at the donor and the acceptor emission wavelengths, 422 and 508 nm, respectively given in Fig. 2c–f. A dramatic change in the QD fluorescence lifetime was noted while changing the GFP concentration and keeping the QD concentration the same, which points at an efficient nonradiative energy transfer from QDs to GFP. Starting with the A/D concentration ratio of 0.96, we observed the photoluminescence decays getting faster with increasing A/D ratio up to 32.6, where we observed adsorption saturation.

The lifetime modification kinetics of both the donor and acceptor with respect to any change of any given FRET pair was found to follow a biexponential behaviour. The lifetime of the donor changes from 10.33 to 2.91 ns as we increase the A/D concentration ratio. Similarly, we carried out the lifetime measurements for the acceptor molecules, where a dramatic increase in the acceptor lifetime was observed because of the energy feeding from the donor to the acceptor. Throughout the A/D ratios we explored, an increase in the acceptor lifetime was observed. We measured lifetime modifications ranging from 3.57 to 4.67 ns for the GFP (the bare lifetime of the GFP, 3.11 ns, is shown with the dotted line in Fig. 2f). The trend of the modification of the lifetime is as expected due to the fact that as we increase the acceptor to donor concentration, we decrease the energy transferred per acceptor, thus the system is evolving to acceptor only case, which is in agreement with the experimental observation.

The observed FRET efficiency due to the dipole interaction of the donor–acceptor pairs was calculated using eqn (2)

$$\eta = 1 - \frac{\tau_{DA}}{\tau_D} \tag{2}$$

where τ_{DA} is the lifetime of the donor in the presence of the acceptor and τ_D is the bare lifetime of the donor. As a result of the energy transfer, we observed FRET efficiencies of up to 70% for our QD–GFP complex. In connection with the theoretical model based on the dipole–dipole interaction, the efficiency levels are in good agreement with the experimentally observed values. In the theoretical approach, we considered energy transfer from ZnCdSe QDs to multiple GFP molecules under exciton–exciton interaction. Within the simplest rate model, the number of excitons (N_{exc}) generated in the QD, under constant illumination (steady-state condition), is given by:[22]

$$-(\gamma^{D}_{exc} + \gamma^{tot}_{trans})N^{D}_{exc} + I_D = 0 \tag{3}$$

where N^{D}_{exc} is the number of excitons in the donor, I_D is the exciton generation rate due to the light excitation, and $\gamma^{D}_{exc} = \gamma^{D}_{exc,rad} + \gamma^{D}_{exc,non\text{-}rad}$ is the donor exciton recombination rate in the absence of the acceptor. $\gamma^{D}_{exc,rad}$ and $\gamma^{D}_{exc,non\text{-}rad}$ are the radiative and nonradiative decay rates, respectively. $\gamma^{tot}_{trans} = n\gamma_{trans}$ is the total energy transfer rate between the donor and multiple acceptors. n is the number of acceptors and γ_{trans} is the energy transfer between one donor and one acceptor. By substituting into eqn (3), it can be written as:

$$-(\gamma^{D}_{exc} + n\gamma_{trans})N^{D}_{exc} + I_D = 0 \tag{4}$$

One then defines:

$$\gamma^{D}_{DA} = (\gamma^{D}_{exc} + n\gamma_{trans}) \tag{5}$$

where γ^{D}_{DA} is the donor exciton lifetime in the presence of energy transfer. For the energy transfer rate between ZnCdSe QDs and GFP,

$$\gamma_{trans} = \gamma^{D}_{exc}\left(\frac{R_0}{r}\right)^6 \tag{6}$$

where R_0 is the Förster radius for the D–A pair and r is the separation distance between ZnCdSe QDs and GFP. Therefore eqn (5) is given by

$$\gamma^{D}_{DA} = \gamma^{D}_{exc}\left(1 + n\left(\frac{R_0}{r}\right)^6\right) \tag{7}$$

In terms of lifetimes,

$$\tau^{D}_{DA} = \frac{\tau^{D}_{exc}}{1 + n\left(\frac{R_0}{r}\right)^6} \tag{8}$$

Here using experimental data, we extracted the effective distance between the QD–GFP to be 5.49 nm on average, which is reasonable when compared with the QD diameter of 4 nm and GFP diameter of ~3 nm.

The enhancement in the FRET efficiencies does not directly reflect the observed light harvesting enhancement. This is because, as more and more acceptors are introduced, there are more non-radiative channels created for the donor to transfer energy, which results in high FRET efficiencies. On the other side, the light harvesting is optimal up to a certain number of acceptors per given donor (~5:1, for our system). When the A/D ratio is further increased, the amount of light harvesting is decreased, since the system is evolving towards an acceptor only system.

QD–GFP based protease sensor with a thermal ON/OFF switch

The well-established FRET process in the GFP–QD nanocomposite is utilized as a protease sensor with a ON/OFF state temperature switch as shown in Fig. 3a. As the FRET process strongly depends on the distance between the donor and acceptor species, any modification in the distance between the species will be reflected in the lifetime of the donor and acceptor facilitating FRET. In the current QD–GFP system, it is suitable to detect trypsin protease available in the reaction medium. The lifetime of FRET facilitating QDs and GFP was modified upon digestion of the linker between the Histag and GFP through protease activation. Changing the enzyme concentration in solution, we observe that the lifetime of the QD–GFP complex follows a trend of decreasing back to the initial GFP lifetime, as follows from Fig. 3b and d. This enables us to use the enzymatic activity to increase the distance among the donor–acceptor pair and thus control the FRET efficiency (Fig. 3a). As the optimum working condition of the trypsin protease is at 37 °C, below this point through the deactivation of the protease no modification of the lifetime of the acceptor was

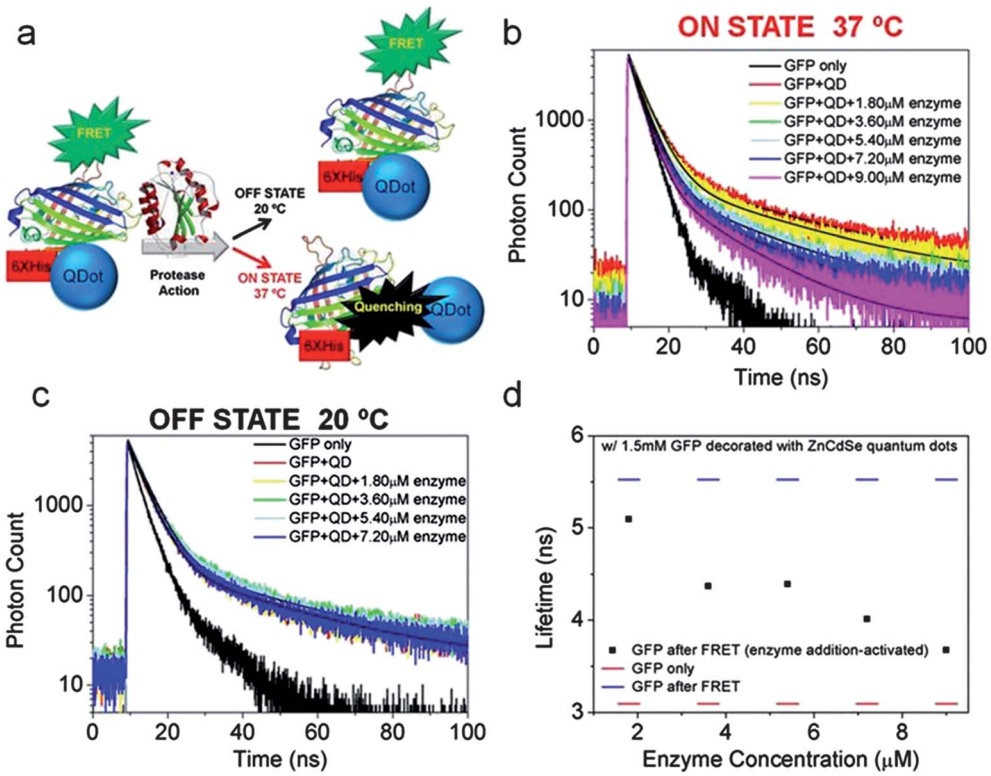

Fig. 3 (a) Schematic representation of the ON/OFF state sensing of the nanohybrid structure in response to the protease action triggered by temperature. (b) Photoluminescence decays of the GFP only, GFP with FRET, and GFP in the ON state of the enzyme. (c) Photoluminescence decays of the GFP only, GFP with FRET, and GFP in the OFF state. (d) Lifetime modifications of the GFP only, GFP with FRET, and GFP after enzyme action.

observed as shown in Fig. 3b. The control experiments were followed in the same manner except for the heat treatment.

Conclusions

We have shown the excitonic composite structures of QD–GFP complexes. The FRET-mediated light harvesting in this composite resulted in up to 15-fold enhancement in the emission of the acceptor protein. The lifetime modifications of the donor–acceptor pair have been supported by the theoretical analysis based on dipole–dipole interaction. Furthermore, the trypsin enzyme was implemented for controlling the energy transfer, breaking the bond in between the QDs and the protein, as a promising tool for the development of the next generation nanosensor coupled with functional proteins. This research area is especially important for showing new functionalities and opportunities for protein-QD based assemblies to be utilized in bioimaging and targeted delivery applications in biomedicine. The capability of tuning the QD fluorescence using the functionalities of the coupled proteins will be useful not only for targeted drug delivery but also for guided diagnostics-treatment.

Cytotoxicity and biological incompatibility are main drawbacks for the utilization of QDs for biological and medical applications.[23] Utilization of QD-photoproteins nanohybrids can overcome this problem. QD–GFP nanohybrids benefit from the biocompatibility of GFP and long fluorescent lifetime of QDs. The QD–GFP nanohybrid could be a promising tool for bioimaging with enhanced functionality. Additionally, the ease of tunability of their biochemical and optical properties through protein engineering makes photoproteins better candidates for coupling with QDs compared to currently available synthetic dyes.

With the current approach ZnCdSe QDs are also shown to be good candidates for the excitation of the photoproteins. One of the most important contributions was made for replacing chemiluminescence to pump a photoprotein with a QD based FRET system. Considering the strong optical emission properties and fluorescence lifetime of QDs, this approach provides an opportunity for a more efficient and flexible emission enhancement for photoproteins. However, there are still challenges including potential toxicity risk induced by the QDs to biological systems and the issue of designing better linkers to control the attachment of photoproteins to QDs.

Hybridization of the photoprotein or other proteins with the nanostructures may enable opportunities to build functional assemblies. Not only the photoproteins but also many enzymes and proteins involved in photo-activated biological events can be tuned and enhanced by using light harvesting nanoparticles.

Acknowledgements

This work was supported by the National Research Foundation of Singapore under Grant no. NRF-CRP-6-2010-2 and NRF-RF-2009-09 and the Singapore Agency for Science, Technology and Research (A*STAR) SERC under Grant no. 112 120 2009. HVD also gratefully acknowledges ESF EURYI and TUBA.

Notes and references

1 T. Miyashiro and E. G. Ruby, *Mol. Microbiol.*, 2012, **84**, 795–806.
2 G. A. Vydryakova, A. A. Gusev and S. E. Medvedeva, *Appl. Biochem. Microbiol.*, 2011, **47**, 293–297.
3 M. T. Nicolas, J. M. Bassot and O. Shimomura, *Photochem. Photobiol.*, 1982, **35**, 201–207.
4 E. A. Widder, *Science*, 2010, **328**, 704–708.
5 J. W. Hastings, *J. Mol. Evol.*, 1983, **19**, 309–321.
6 D. Scott, E. Dikici, M. Ensor and S. Daunert, in *Annual Review of Analytical Chemistry*, ed. R. G. Cooks and E. S. Yeung, Annual Reviews, Palo Alto, 2011, vol. 4, pp. 297–319.
7 R. Borra, D. Z. Dong, A. Y. Elnagar, G. A. Woldemariam and J. A. Camarero, *J. Am. Chem. Soc.*, 2012, **134**, 6344–6353.
8 M. Drobizhev, N. S. Makarov, S. E. Tillo, T. E. Hughes and A. Rebane, *Nat. Methods*, 2011, **8**, 393–399.
9 H. Mizuno, A. Sawano, P. Eli, H. Hama and A. Miyawaki, *Biochemistry*, 2001, **40**, 2502–2510.
10 I. L. Medintz, J. H. Konnert, A. R. Clapp, I. Stanish, M. E. Twigg, H. Mattoussi, J. M. Mauro and J. R. Deschamps, *Proc. Natl. Acad. Sci. U. S. A.*, 2004, **101**, 9612–9617.
11 A. L. Rogach, A. Sukhanova, A. S. Susha, A. Bek, S. Mayilo, J. Feldmann, V. Oleinikov, B. Reveil, B. Donvito, J. H. M. Cohen and I. Nabiev, *Nano Lett.*, 2007, **7**, 2322–2327.
12 E. R. Goldman, I. L. Medintz, J. L. Whitley, A. Hayhurst, A. R. Clapp, H. T. Uyeda, J. R. Deschamps, M. E. Lassman and H. Mattoussi, *J. Am. Chem. Soc.*, 2005, **127**, 6744–6751.
13 A. M. Dennis and G. Bao, *Nano Lett.*, 2008, **8**, 1439–1445.
14 V. R. Hering, G. Gibson, R. I. Schumacher, A. Faljoni-Alario and M. J. Politi, *Bioconjugate Chem.*, 2007, **18**, 1705–1708.
15 A. Rakovich, A. Sukhanova, N. Bouchonville, E. Lukashev, V. Oleinikov, M. Artemyev, V. Lesnyak, N. Gaponik, M. Molinari, M. Troyon, Y. P. Rakovich, J. F. Donegan and I. Nabiev, *Nano Lett.*, 2010, **10**, 2640–2648.
16 I. Nabiev, A. Rakovich, A. Sukhanova, E. Lukashev, V. Zagidullin, V. Pachenko, Y. P. Rakovich, J. F. Donegan, A. B. Rubin and A. O. Govorov, *Angew. Chem., Int. Ed.*, 2010, **49**, 7217–7221.
17 U. O. S. Seker, T. Ozel and H. V. Demir, *Nano Lett.*, 2011, **11**, 1530–1539.
18 V. Lesnyak, A. Plotnikov, N. Gaponik and A. Eychmuller, *J. Mater. Chem.*, 2008, **18**, 5142–5146.
19 U. O. S. Seker, G. Zengin, C. Tamerler, M. Sarikaya and H. V. Demir, *Langmuir*, 2011, **27**, 4867–4872.
20 E. Yuca, A. Y. Karatas, U. O. S. Seker, M. Gungormus, G. Dinler-Doganay, M. Sarikaya and C. Tamerler, *Biotechnol. Bioeng.*, 2011, **108**, 1021–1030.
21 Y. M. Wang, J. O. Tegenfeldt, W. Reisner, R. Riehn, X. J. Guan, L. Guo, I. Golding, E. C. Cox, J. Sturm and R. H. Austin, *Proc. Natl. Acad. Sci. U. S. A.*, 2005, **102**, 9796–9801.
22 E. Mutlugun, P. L. Hernandez-Martinez, C. Eroglu, Y. Coskun, T. Erdem, V. K. Sharma, E. Unal, S. K. Panda, S. G. Hickey, N. Gaponik, A. Eychmuller and H. V. Demir, *Nano Lett.*, 2012, **12**, 3986–3993.
23 F. M. Winnik and D. Maysinger, *Acc. Chem. Res.*, 2013, **46**, 672–680.